Revista Mexicana de Astronomía y Astrofísica, **33**, 73–81 (1997)

THE BOW SHOCK AND H II REGION AROUND A RUNAWAY O STAR

A. C. Raga[1], A. Noriega-Crespo[2], J. Cantó[1], W. Steffen[3],
D. Van Buren[2], G. Mellema[4], and P. Lundqvist[4]

Received 1997 March 3; accepted 1997 May 10

RESUMEN

Las estrellas O de alta velocidad, tienen velocidades peculiares de $\sim$ 30–100 km s^{-1}. Estas estrellas pasan a través del plano galáctico, interactuando con el medio interestelar circundante. Esta interacción produce dos tipos de estructura: una región H II y un choque a proa. Los choques a proa tienen tamaños característicos de $\sim$ 1–5 pc y son observados mayormente en el infrarrojo lejano. Las regiones H II tienen tamaños característicos mucho mayores, de $\sim$ 100 pc, de forma que rodean al choque a proa completamente.

Presentamos simulaciones axisimétricas detalladas tanto de la región H II como del choque a proa, de una estrella O5 viajando a una velocidad de 100 km s^{-1} a través de un medio ambiente neutro y homogéneo, de una densidad $n = 1$ cm^{-3} Las características de la interacción estrella/medio ambiente son descritas en detalle y también se presentan predicciones de las propiedades observacionales (tanto en longitudes ópticas como infrarrojas).

ABSTRACT

Runaway O stars have high peculiar velocities of $\sim$ 30–100 km s^{-1}. These stars flow through the galactic plane, and interact with the surrounding ISM. This interaction produces two types of structure: an H II region and a stellar wind bow shock. The bow shocks have characteristic sizes of $\sim$ 1–5 pc, and are observed mostly in the far IR. The H II regions have much larger characteristic sizes of $\sim$ 100 pc, completely enveloping the bow shock.

We present detailed axisymmetric radiation gasdynamic numerical simulations of both the H II region and the stellar wind bow shock of an O5 star, moving at a velocity of 100 km s^{-1} through a homogeneous, neutral environment of density $n =$ 1 cm^{-3}. The characteristics of the star/environment interaction are described in detail, and predictions of observable quantities (in both optical and IR wavelengths) are carried out.

Key words: **H II REGIONS — SHOCK WAVES**

1. INTRODUCTION

Runaway O stars streaming through the galactic plane at large ($\sim$ 30–100 km s^{-1}) velocities generate two flow structures: *(i)* an outer, cometary H II region, and *(ii)* an inner stellar wind bow shock.

Approximate models for the H II region have been constructed in the past by Thuan (1975) and Raga (1986). The bow shock has been modeled (using a thin shell formulation) by Van Buren & Mac Low (1992) in the context of ultracompact H II regions, and by Dgani, Van Buren & Noriega-Crespo (1996) for OB runaway stars. An exact solution of the thin shell problem was derived by Wilkin (1996). Numerical simulations of a supersonic stellar wind interacting with a uniform streaming flow, in the adiabatic regime and at low resolution, have been carried out by Matsuda et al. (1989). In the present paper, we discuss a full numerical simulation (including a treatment of the gas dynamical and radiative transfer processes) of such a flow.

[1] Instituto de Astronomía, Universidad Nacional Autónoma de México.
[2] Infrared Processing and Analysis Center, USA.
[3] Department of Physics and Astronomy, U. of Manchester, UK.
[4] Stockholm Observatory, Sweden.

To this effect, we have first included a treatment of the transfer of the stellar, ionizing radiation in the gasdynamic/microphysical code described by Raga, Mellema, & Lundqvist (1997). This is described in detail in § 2. We have then used the code to model the outer H II region (§ 3) and the inner, stellar wind bow shock (§ 4). The computed flow stratifications are then used to compute Hα and IR dust continuum intensity maps.

These results are of particular interest in terms of the *IRAS* observations of bow shocks around runaway O stars (Van Buren, Noriega-Crespo, & Dgani 1995; Noriega-Crespo, Van Buren, & Dgani 1997). Wind driven bow shocks are promising laboratories to study the physics of shock interactions, the properties of the dust-to-gas ratio and the dust emissivity in relatively low density environments (~ 1 cm^{-3}). A detailed comparison between these observations and the theoretical models will be presented in a future paper.

2. THE RADIATIVE TRANSFER SCHEME

We have used the axisymmetric, adaptive grid Coral gasdynamic code in order to obtain self-consistent models of the interaction of the radiation field and stellar wind from an O star with a neutral environment. The version of the code that we have used, incorporates a number of ionization states of different elements (H, N, O, S and Ne), computing both the non-equilibrium rate equations and the cooling rates (due to collisional line excitation and other processes) as described in detail by Raga et al. (1997). To this code, we have now added a treatment of the transfer of ionizing radiation emitted by a point source located on the symmetry axis, and incorporated the photoionization rates in the ionization rate-of-change equations, together with the corresponding term in the energy equation.

The transfer of ionizing radiation is computed in the following, approximate way. We first compute a column density of neutral hydrogen

$$N = \int_0^R n_{HI} dR' \,, \tag{1}$$

for radial directions joining all of the grid points with the photon source. Computing these radial integrals in the cylindrical, adaptive grid of the Coral code of course requires a non-trivial numerical scheme, which we do not describe in detail.

The photoionization rates for all species k are then calculated as

$$\phi_k = \left(\frac{R_*}{R}\right)^2 e^{-\tau} \, \phi_{k,0} \,, \tag{2}$$

where

$$\phi_{k,0} = \int_{\nu_k}^{\infty} \frac{\pi F_\nu}{h\nu} \sigma_k(\nu) d\nu \,, \tag{3}$$

is the photoionization rate per particle of species k at the stellar radius R_*. In equation (3), F_ν is the stellar ("astronomical") flux, $\sigma_k(\nu)$ is the photoionization cross section, and ν_k is the ionization limit of species k. The photoionization rates per unit volume $n_k \phi_k$ are then incorporated into the appropriate ionization rate-of-change equations (see Raga et al. 1997). We should note that the $1/R^2$ geometrical dilution for the radiative flux used in equations (2) and (3) is entirely appropriate for the simulations described in the present paper, as the spatial resolution of the highest resolution simulations is ~ 5 orders of magnitude coarser than the radius of the photoionizing O5 star.

In taking the optical depth out of the integral in equation (2), we are neglecting the hardening of the spectrum that occurs close to the ionization front. This approximation simplifies the computation in a considerable way, since it allows us to calculate the frequency integrals (equation 3) ahead of carrying out the numerical simulation (instead of recalculating them for different times and spatial positions).

The frequency-independent optical depth τ (see eq. 2) is calculated as $\tau = N \, \overline{\sigma}$, where the average hydrogen photoionization cross-section $\overline{\sigma}$ is given by

$$\overline{\sigma} = \frac{4\pi {R_*}^2 \phi_{H,0}}{S} \,, \tag{4}$$

where $\phi_{H,0}$ is the photoionization rate of hydrogen (see eq. 3) at the surface of the star, and

$$S = 4\pi {R_*}^2 \int_{\nu_H}^{\infty} \frac{\pi F_\nu}{h\nu} d\nu \,, \tag{5}$$

is the total number of ionizing photons emitted by the star. In choosing the average absorption coefficient in this way (see eq. 4), we ensure that the size of an H II region computed with our monochromatic radiative transfer coincides with the size of the appropriate Strömgren sphere.

Analogously, we compute the energy gain (per atom) due to ionization of hydrogen as

$$\psi_H = \left(\frac{R_*}{R}\right)^2 e^{-\tau} \, \psi_{H,0} \,, \tag{6}$$

where

$$\psi_{H,0} = \int_{\nu_H}^{\infty} \frac{\pi F_\nu}{h\nu} (h\nu - h\nu_H) \sigma_H(\nu) d\nu \,, \tag{7}$$

and incorporate the energy gain per unit volume $n_{HI} \psi_H$ into the energy equation.

Neglecting the hardening of the spectrum results in an incorrect structure for the transition within the ionization fronts. However, in the numerical simulations presented in this paper, the ionization fronts are unresolved, so this is not an important problem. On the other hand, the optically thin region between the source and the ionization front is correctly described with our simplified radiative transfer treatment. Needless to say, we do not explicitly compute the transfer of diffuse ionizing radiation.

We should also note that in the models of Raga et al. (1997), helium was omitted because it does not contribute significantly to the radiative cooling. In the present models, where we include photoionization, helium is more important since it adds to the heating of the gas, as well as absorbs a major part of the photons with energy > 24.6 eV. However, considering the approximate treatment of the radiative transfer described above, we have also omitted helium in the present models. Models with a treatment of the ionization state of helium, together with a treatment of the hardening of the spectrum, will be presented in a subsequent paper.

3. THE H II REGION

Let us consider an O5 star (of effective temperature $T_{eff} = 50\,000$ K, radius $R_* = 9.8 \times 10^{11}$ cm and an ionizing photon rate $S = 6.16 \times 10^{49}$ s^{-1}) moving at a velocity of $v = 100$ km s^{-1} through a homogeneous, neutral medium of number density $n = 1$ cm^{-3}. For the neutral environment, we assume a temperature of 300 K (though the precise value of this temperature is unimportant for the numerical simulation). For the stellar flux, we take the values from the models calculated for hot main sequence stars by Kurucz (1969). With the appropriate flux, we then compute the integrals of equations (3), (4) and (7), which allow us to incorporate the effects of the ionizing radiation field into our numerical gasdynamic simulation.

It is expected that the ionization front surrounding the H II region produced by the O star will not be spherical, as a result of the highly supersonic motion of the star with respect to the surrounding medium. It is possible to compute the separation between the star and the ionization front in the upstream direction (i.e., in the direction of motion of the star) as follows.

From a simple "Strömgren region" argument of balance between emitted ionizing photons and photoionizations per unit time, we see that for a solid angle $\Delta\Omega$ centred on the direction of motion of the star, we have

$$S\,\frac{\Delta\Omega}{4\pi} = \dot{N}_{rec} + \dot{N}_{in}\,, \tag{8}$$

where $S\,\Delta\Omega/(4\pi)$ is the rate of ionizing photons emitted by the star into the solid angle $\Delta\Omega$,

$$\dot{N}_{rec} = \frac{1}{3} R_0{}^3 n_0^2 \alpha\,\Delta\Omega\,, \tag{9}$$

is the total rate of recombinations occurring within $\Delta\Omega$, and

$$\dot{N}_{in} = n_0\, v_0\, R_0{}^2\,\Delta\Omega\,, \tag{10}$$

is the total rate of neutrals being fed into the ionized region through the ionization front as the star travels at speed v_0. From equations (8–10), we see that the separation R_0 between the source and the ionization front (in the direction of the motion of the star) is given by the equation

$$\left(\frac{R_0}{R_S}\right)^3 + \xi \left(\frac{R_0}{R_S}\right)^2 = 1\,, \tag{11}$$

where the Strömgren radius R_S is given by the usual expression, and $\xi = (3v_0)/(\alpha n_0 R_S)$. Using the parameters given at the beginning of this section, and a hydrogen recombination coefficient $\alpha = 4.18 \times 10^{-13}$ cm^3 s^{-1} (at 10^4 K), we obtain $R_S = 3.28 \times 10^{20}$ cm, $\xi = 0.22$ and $R_0 = 0.93\,R_S$ (from equation 11). In other words, the effect of the motion of the star with respect to the surrounding medium is to reduce the separation between the star and the ionization front (in the upstream direction) by a factor of 0.93 with respect to the radius of a stationary Strömgren sphere. Somewhat larger values for R_S and R_0 are obtained by using the case B recombination coefficient for hydrogen, which is $\alpha = 2.59 \times 10^{-13}$ cm^3 s^{-1} at 10^4 K. The numerical simulation shown below is computed with the case A hydrogen recombination coefficient.

From similar arguments, it is also possible to derive a simple differential equation for the shape of the ionized region (i.e., not only deriving the size of the region in the upstream direction). This has been done by Raga (1986), who computed numerical solutions of the resulting differential equation, but was unable to find an analytic solution. There is, however, a simple approximate solution. The differential equation can be written as

$$\left(\frac{R}{R_S}\right)^3 + \xi \left(\frac{R}{R_S}\right)\left[\left(\frac{\dot{R}}{R_S}\right)\sin\theta + \left(\frac{R}{R_S}\right)\cos\theta\right] = 1\,, \tag{12}$$

which for $\xi \ll 1$ has the approximate solution

$$R \approx R_S(1 - \xi\,\cos\theta)^{1/3}\,. \tag{13}$$

The angle θ is measured from the symmetry axis of the configuration, and $\dot{R}$ (in eq. 12) indicates a

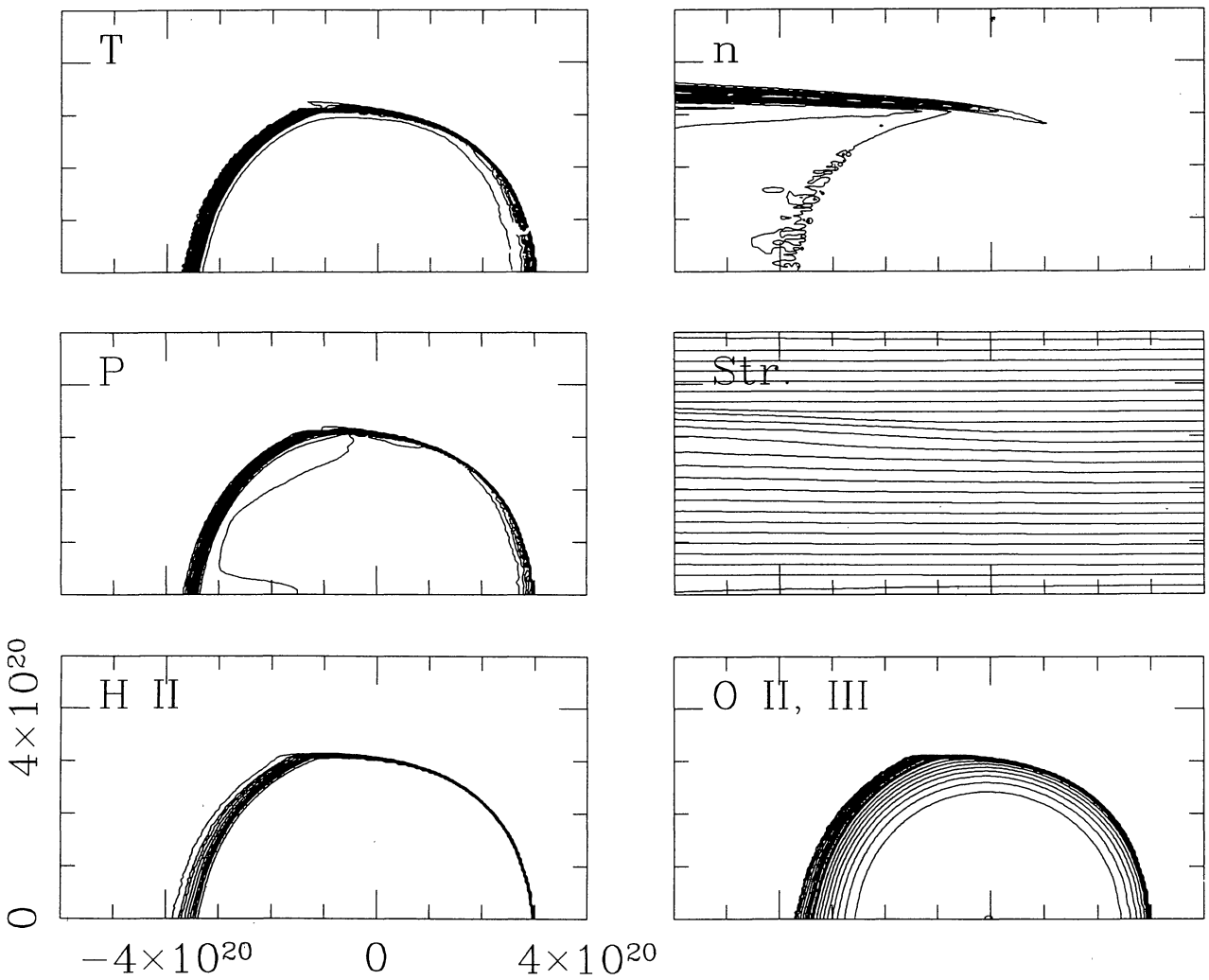

Fig. 1. Stratification of the stationary H II region produced by the passage of an O5 star through a homogeneous environment over a 4 by 8 × 10^{20} cm region (the parameters of the model are described in the text). The graph shows the temperature stratification (top left, linear contours in steps of 500 K), the pressure stratification (centre left, linear contours in steps of 2 × 10^{-13} erg cm^{-2}), the ionization fraction of hydrogen (bottom left, linear contours in steps of 0.1), the ion+atom number density (top right, linear contours in steps of 0.2 cm^{-3}), the streamlines of the flow (centre right) and the O II (dashed contours) and O III (solid contours) ionization fractions (bottom right, linear contours in steps of 0.1 for both ionization fractions).

derivative with respect to θ. This solution can be compared with the one we present below, which is derived from the full radiative transfer/gasdynamic problem of the H II region produced by the high velocity O star.

The radiative transfer + photoionization problem has already been solved numerically by Thuan (1975). This calculation was done under the assumption that the highly supersonic motion of the O star results in a photoionized region with an "unperturbed" density (i.e., that the density within the ionized region is homogeneous and identical to the density of the unperturbed, neutral environment). This assumption is, of course, shared by our simple, Strömgren region approach described above (and also used by Raga 1986).

Figure 1 shows the stratification of the stationary configuration attained by the flow produced by an O5 star moving at a velocity $v_0 = 100$ km s^{-1}, with respect to a neutral, $n_0 = 1$ cm^{-3} environment. The stationary configuration was obtained after a time-integration of $\sim 10^6$ yr. This timescale is compa-

rable to both the lifetime of the O5 star, and to the timescale in which it crosses the height of the galactic plane. Because of this, the stationary configuration might not be attained by actual runaway O5 stars. However, the calculations of Thuan (1975) show that the nonstationary regime (corresponding to an O star passing through the plane of the galaxy), produces cometary H II regions with structures which are qualitatively similar to the stationary solutions (see also Raga 1986).

A sharp, hydrogen ionization front is formed ahead of the star (see Figure 1), at a distance from the source that agrees well with the prediction from the Strömgren analysis described above (see eq. 11). In the downstream direction, a more diffuse "recombination front" is formed. Higher ionization species are found in the region close to the star. In Figure 2, we show a comparison between the approximate analytic solution (13), a numerical solution of equation (12), and the shape for the H II region (as defined by the contour of 50 % hydrogen ionization). A reasonably good agreement is found for the predicted shapes of the H II region.

The temperature stratification (see Figure 1) shows a sharp ionization front (in the leading hemisphere), and a more diffuse recombination front (in the trailing hemisphere) surrounding a quite precisely isothermal (with temperatures of $\approx$ 9050 $\pm$ 50 K) H II region. The density stratification (Fig. 1), confirms that most of the H II region actually does have basically the same density as the unperturbed, neutral environment. However, we find that the "wings" of the ionization front actually do produce a substantial compression. This can be understood in the following way.

In the "head" of the H II region (i.e., in the region directly upstream of the star), the ionization front moves with respect to the surrounding, neutral medium at a velocity of $\approx$ 100 km s^{-1} which is highly supersonic with respect to both the sound speed $c_n \sim 2$ km s^{-1} of the neutral gas and the sound speed $c_I \sim 10$ km s^{-1} of the ionized gas, and is thus an ionization front of the R (weak) type. The density behind the ionization front is only slightly higher than the pre-front density. As one moves along the ionization front towards the "wings" of the H II region, the normal velocity of the ionization front relative to the neutral medium decreases, until it falls to a value of twice c_I. At this point the ionization front becomes R-critical and the post-front density reaches a value of $\sim$ twice the pre-front density. Further along the ionization front its normal velocity relative to the neutral medium is even smaller and a shock front must precede the ionization front. This shock allows the ionization front to smoothly become a D-type front. For the parameters considered in this paper the shape of the H II region is almost spherical, and thus the velocity of the ionization front is approximately given by $v_i \approx v_0 \cos\theta$. Taking $v_i = 20$ km s^{-1} and $v_0 = 100$ km s^{-1}, then $\theta = 78.^\circ5$, which compares well with the point where the results of the simulation show an increase in the density across the ionization front (see Fig. 1).

In our numerical simulation (see Fig. 1), we observe that the gas that is compressed in the wings of the H II region forms a confined trail of neutral material. Such trails might be observable as features in the IR continuum re-radiated by the dust grains. To our knowledge, such features have never been seen. These features are clearly seen in Figure 3, where we show predicted Hα and dust continuum maps. The Hα intensity coefficient has been computed considering the contributions from both collisional excitations and the recombination cascade, and the dust continuum emission coefficient is computed (in the Rayleigh-Jeans limit) as

$$j_{\nu,dust} = \frac{\pi < r_g{}^2 > \nu^2 k}{2c^2} T_{dust} f_{dust} n_H \; ; \qquad (14)$$

where ν is the frequency at which the observation is carried out, c and k are the speed of light and the Boltzmann constant (respectively), $< r_g{}^2 >$ is the average mean square radius over the grain distribution, n_H is hydrogen number density, and f_{dust} is the dust-to-hydrogen number ratio. We take the dust temperature T_{dust} to be given by

$$T_{dust} = \left(\frac{L}{16\pi R^2 \sigma} \right)^{1/4} \; ; \qquad (15)$$

where L is the luminosity of the star (assumed to be dominated by the unattenuated stellar radiation longwards of the Lyman limit), R is the distance from

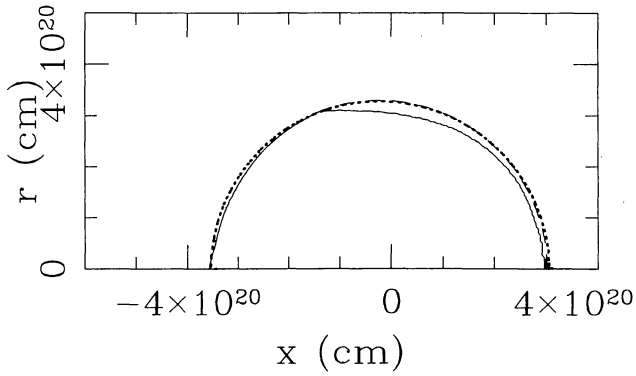

Fig. 2. Comparison between the analytic and numerical calculations of the shape of the H II region. The thin line shows the contour of 50 % hydrogen ionization obtained from the numerical simulation (see the text and Fig. 1). The thick line corresponds to the approximate, analytic solution (equation 13) overplotted on a numerical integration of equation (12). The differences between the two solutions are not visible in the plot.

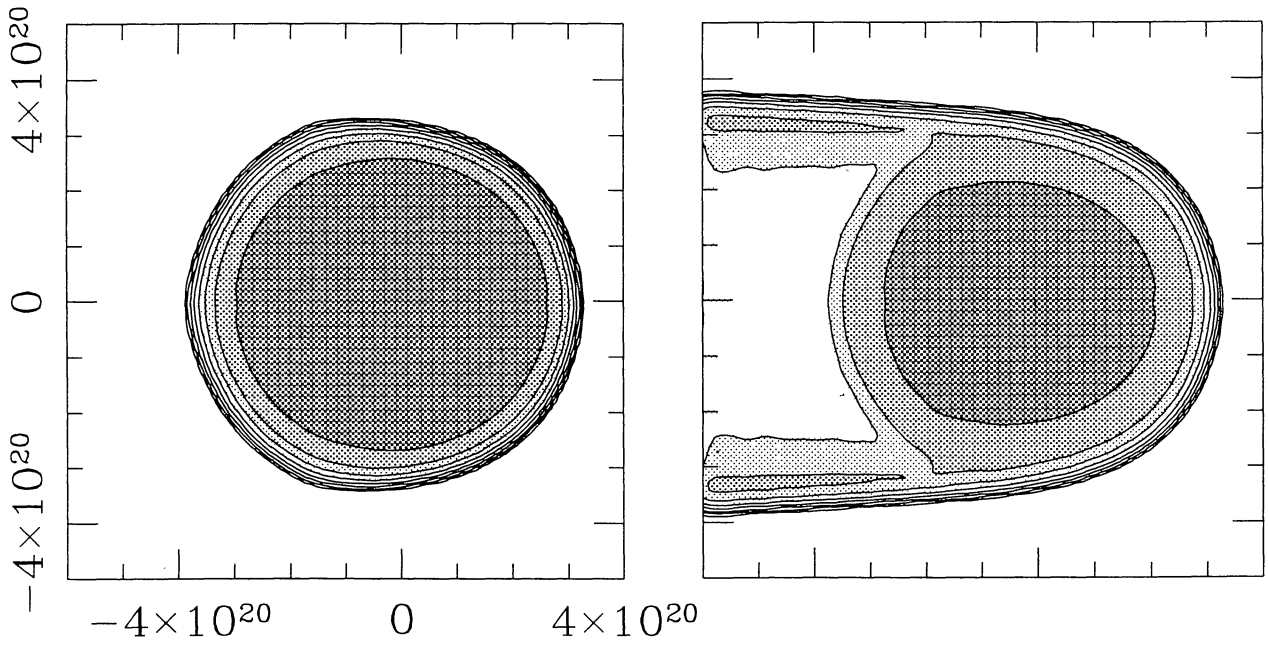

Fig. 3. Hα (left) and dust continuum (right) images computed from the H II region model (see the text and Fig. 1), assuming that the flow axis lies in the plane of the sky. The contours are logarithmic, with two successive contours corresponding to a factor of 2. A greyscale is also shown, so as to indicate the positions of the local maxima.

the source, and σ is the Stefan-Boltzmann radiation constant. This simple relation is obtained by considering the dust temperature to be determined from the balance between the impinging stellar radiation and the IR continuum emitted by the dust grains.

With these calculations of the Hα and dust continuum emission coefficients, through a straightforward integration through lines of sight, we obtain the maps shown in Fig. 3. The Hα map shows a homogeneous, slightly elongated H II region, with a centre that is offset from the position of the ionizing star. The dust continuum map shows both the H II region and an elongated "tail", coming from the emission of the compressed zone resulting from the D-type fronts obtained for polar angles $\theta > 78°.5$ (see above and Fig. 1).

We should discuss an apparent discrepancy between our results and the work of Thuan (1975). In this work, simple arguments about the expansion of an H II region around a moving source are used to show that the formation of shocks has to be limited to a confined region directly *behind* the star. However, these arguments are based on the assumption that the ionization front travels out from the star at a time- and direction-independent velocity. This assumption would only apply for the very early expansion of the H II region (immediately following the "turning on" of the central star), so that the formation of shocks in a more evolved situation cannot be described with this formalism. In this way, we see that the apparent discrepancy between our results and the description of Thuan (1975) is only a result of the different regimes which are studied.

4. THE STELLAR WIND BOW SHOCK

More interesting from an observational point of view is the bow shock created by the interaction between the O star wind and the environment which is streaming by. This interaction has been studied analytically by Dyson (1975, who found an analytic solution to the ram pressure balance problem), by Wilkin (1996, who found an analytic solution which includes centrifugal effects) and by Cantó, Raga, & Wilkin (1996, who reduced the solution method to an algebraic equation when conservation of angular momentum is considered). Van Buren & Mac Low (1992) carried out numerical integrations of this "thin shell" problem. These calculations apply to the runaway O star problem only in an approximate way, since in this problem the shocked stellar wind will behave adiabatically, so that the shocked region will not be very thin.

From the standard, ram pressure balance argument, one sees that the upstream standoff distance between the bow shock and the star is

$$R_{bs} = \left(\frac{\dot{M}\, v_w}{4\pi\, n\, m\, v^2} \right)^{1/2}, \qquad (16)$$

where $\dot{M}$ is the mass loss rate and v_w the (constant) velocity of the stellar wind, n is the number density of atoms and ions, m the average mass per ion or atom, and v is the relative velocity between the star and the surrounding environment.

For an O5 star with $\dot{M} = 6 \times 10^{-5}$ $M_\odot$ yr^{-1} and $v_w = 3000$ km s^{-1} moving at a velocity $v = 100$ km s^{-1} inside a $n = 1$ cm^{-3} environment, from equation (16) we obtain a bow shock standoff distance $R_{bs} = 2.05 \times 10^{19}$ cm. This distance is more than an order of magnitude smaller than the size (in the upstream direction) $R_0 = 2.69 \times 10^{20}$ cm of the H II region around the O star (see the previous section). From these estimates, we conclude that the stellar wind bow shock will be lying within the central zone of the H II region computed in the previous section (see Fig. 1).

We therefore carry out a numerical simulation in which we have an O5 star with the wind parameters described above (and the ionizing radiative field discussed in the previous section) moving at a velocity $v_0 = 100$ km s^{-1} in an ionized medium of number density $n_0 = 1$ cm^{-3} (of ions and atoms). We assume that the O star wind is completely ionized (in our scheme which only considers up to 6 ionization states), and that the environment has a temperature $T_e = 10^4$ K and an ionization state with H II, C III, O III, S III and Ne III. This is consistent with the ionization structure found for the central zone of the H II region computed in the previous section. For the numerical simulation, we use a 4-level binary adaptive grid with a maximum resolution (in both axial and radial directions) of 2.93×10^{17} cm.

We find that the flow never attains a stationary configuration, but that after a timescale $\sim 2 \times 10^5$ yr it does achieve a "statistically stationary" regime. The flow stratification obtained after a time integration of 3.4×10^5 yr is shown in Figure 4. From the pressure stratification, we clearly see the two-shock stellar wind/environment interaction structure. In both the density and temperature contour plots, we also see the contact discontinuity that separates the hot ($\sim 1.5 \times 10^8$ K), low density ($\sim 6 \times 10^{-3}$ cm^{-3}) post-wind shock gas from the comparatively cool ($\sim 3 \times 10^4$ K), high density (~ 10 cm^{-3}) post-bow shock gas, where the values quoted correspond to

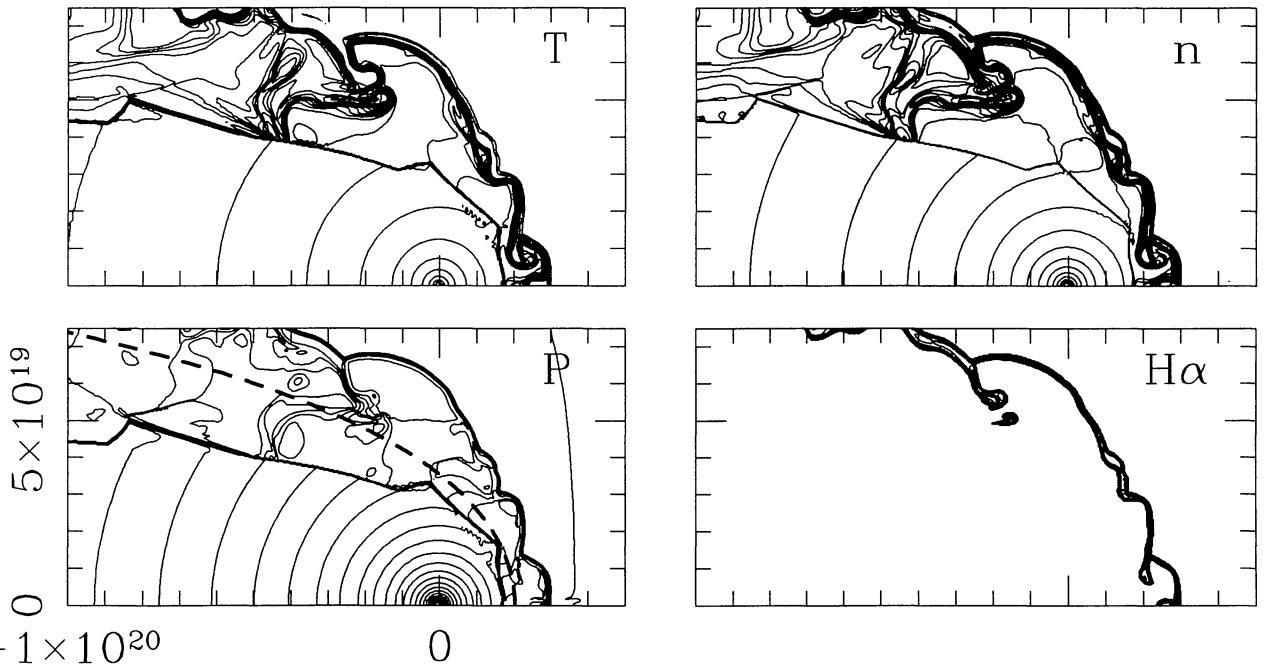

Fig. 4. Stratification of the stellar wind bow shock resulting from the passage of an O5 star through a homogeneous environment (the parameters of the model are described in the text). The graph shows the temperature stratification (top left), the pressure stratification (bottom left), the ion+atom number density (top right), and the Hα emission coefficient (bottom right). The four graphs show logarithmic, factor of 2 contours. In the pressure plot (bottom left) we have also plotted the analytic, thin shell solution (for the appropriate parameters) of Wilkin (1996) for the shape of the stellar wind bow shock (dashed line).

the stagnation region. The stagnation region standoff distance between the two shocks has a value of $\approx 1.3 \times 10^{19}$ cm, so that it is resolved with approximately 44 grid points.

The flow structure is quite complex, with an unstable, cool, thin shell formed by the post-bow shock material (see Fig. 4). This cool layer twists into "tongues" of material which are then swept back by the flow. The inner wind shock is more steady, being cushioned from the highly unstable post-bow shock shell by a hot bubble of shocked wind material. This adiabatic bubble results in a considerable separation between the wind and bow shocks, so that a "thin shell" approximation is not valid for computing the loci of the shocks. We have anyway plotted the analytic, thin shell solution of Wilkin (1996) on the pressure plot of Fig. 4. From this graph, it is clear that while the numerical simulation does not result in the formation of a thin shell, the flow still qualitatively resembles the solution of Wilkin (1996).

From the flow stratification shown in Fig. 4, we have computed the Hα and dust continuum maps (see § 3). These maps (see Figure 5) show that the Hα emission is more concentrated towards the head of the bow shock, while the dust continuum has more extended emission in the bow shock wings.

5. CONCLUSIONS

In this paper, we have studied the problem of the interaction between a runaway O star and the surrounding environment. In order to do this, we have first included a treatment of the transfer of ionizing radiation (§ 2) in the gasdynamic code described by Raga et al. (1997).

We have then carried out a numerical simulation for the case of an O5 star streaming past a neutral environment (of density $n = 1$ cm^{-3}) at a velocity of 100 km s^{-1}. The resulting flow has an outer H II region (described in § 3) of diameter $\sim 6 \times 10^{20}$ cm (see Fig. 1) and an inner stellar wind bow shock of diameter $\sim 10^{20}$ cm (measured perpendicular to the direction of motion, see Fig. 4 and § 4).

We have derived an approximate, "Strömgren region" analytic description of the outer H II region (§ 3) and find that it approximately reproduces the results from the full numerical simulation (Fig. 2). We have also compared the analytic, thin shell solution of Wilkin (1996) with the numerical simulation of the inner bow shock. We find that even though the numerical simulation does not produce a thin shell flow (due to the fact that the stellar wind shock is adiabatic), a partial, qualitative agreement is still obtained between the analytic and numerical calculations.

The most unexpected prediction from our numerical simulation is that the H II regions around runaway O stars should have long "tails" of neutral, dense material. These tails are produced by the shocks associated with the D-type ionization fronts produced along the sides of the H II region. We pro-

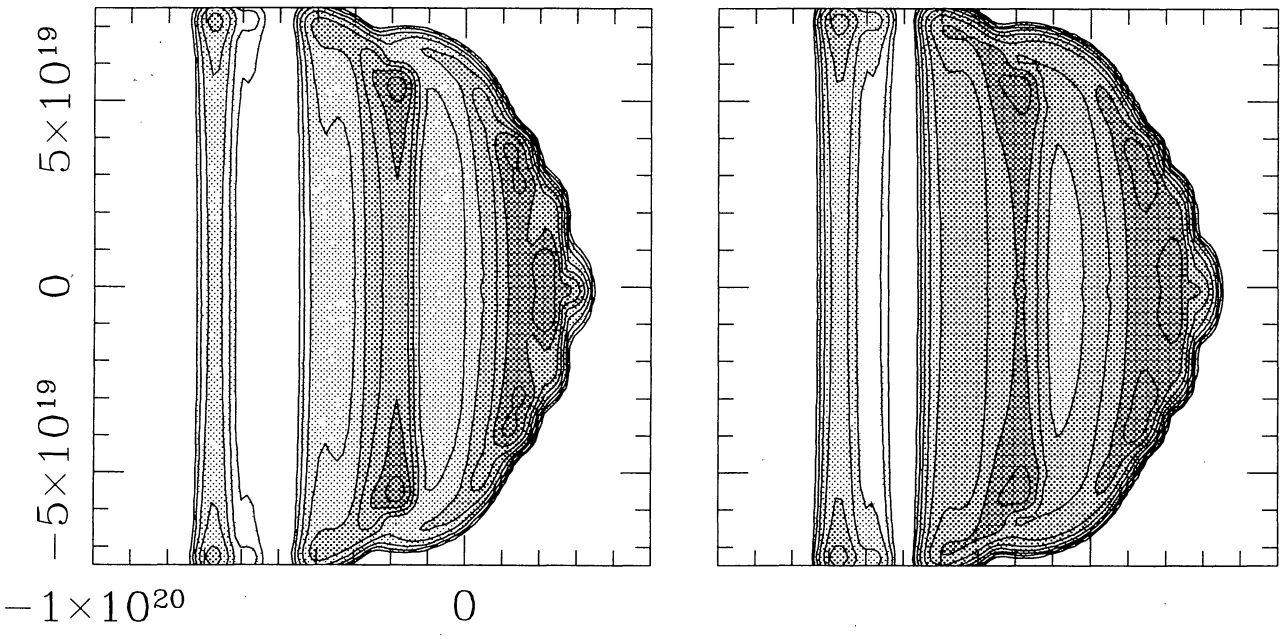

Fig. 5. Hα (left) and dust continuum (right) images computed from the stellar wind bow shock simulation (see the text and Fig. 4), assuming that the flow axis lies in the plane of the sky. The contours are logarithmic, with two successive contours corresponding to a factor of 2. A greyscale is also shown, so as to indicate the positions of the local maxima.

pose that these tails might be observed in the IR dust continuum observed with *IRAS*.

In a second paper, we will present detailed comparisons between numerical simulations and optical and IR observations of H II region/bow shock structures around runaway O stars.

We would like to thank an anonymous referee for most helpful comments about this paper. ANC, WS and GM thank the IAUNAM for a very pleasant stay in Mexico City, during the completion of this work. AR and JC acknowledge support from CONACYT, DGAPA (UNAM) and the UNAM/Cray research program. ANC's research is supported by NASA Long Term Astrophysics Program through JPL under contract with the California Institute of Technology. WS acknowledges support by a PPARC research associateship.

REFERENCES

Cantó, J., Raga, A. C., & Wilkin, F. P. 1996, ApJ, 469, 729
Dgani, R., Van Buren, D., & Noriega-Crespo, A. 1996, ApJ, 461, 927
Dyson, J. E. 1975, Ap&SS, 35, 299
Kurucz, R. 1969, in Theory and Observation of Normal Stellar Atmospheres: Proceedings of the Third Harvard-Smithsonian Conference on Stellar Atmospheres, ed. O. Gingerich (Massachusetts: MIT Press), 401
Matsuda, T., Fujimoto, Y., Shima, E.; Sawada, K., & Inaguchi, T. 1989, ProTheoPhys, 81, 810
Noriega-Crespo, A., Van Buren, D., & Dgani, R. 1997, AJ, 113, 780
Raga, A. C. 1986, ApJ, 300, 745
Raga, A. C., Mellema, G., & Lundqvist, P. 1997, ApJS, 109, 517
Thuan, T. X. 1975, ApJ, 198, 307
Van Buren, D., & Mac Low, M. M. 1992, ApJ, 394, 534
Van Buren, D., Noriega-Crespo, A., & Dgani, R. 1995, AJ, 110, 2914
Wilkin, F. P. 1996, ApJ, 459, L31

Jorge Cantó and Alejandro C. Raga: Instituto de Astronomía, UNAM, Apartado Postal 70-264, 04510 México, D.F., México. (raga@astroscu.unam.mx).
Peter Lundqvist and Garrelt Mellema: Stockholm Observatory, S-133 36, Saltsjöbaden, Sweden.
Alberto Noriega-Crespo and D. Van Buren: Infrared Processing and Analysis Center, M/S 100-22, California Institute of Technology, 770 So. Wilson Ave., Pasadena, CA 91125, USA.
W. Steffen: Department of Physics and Astronomy, University of Manchester, Oxford Rd., Manchester M13 9PL, UK